

**Finite-temperature lattice dynamics and superionic transition in ceria from first principles**Johan Klarbring,<sup>1,\*</sup> Natalia V. Skorodumova,<sup>2,3</sup> and Sergei I. Simak<sup>1</sup><sup>1</sup>*Department of Physics, Chemistry and Biology (IFM), Linköping University, SE-581 83, Linköping, Sweden*<sup>2</sup>*Materials Science and Engineering Department, KTH-Royal Institute of Technology, Brinellvägen 13, 10044 Stockholm, Sweden*<sup>3</sup>*Department of Physics and Astronomy, Uppsala University, Box 516, 751 20 Uppsala, Sweden*

(Received 5 January 2018; revised manuscript received 23 February 2018; published 21 March 2018)

*Ab initio* molecular dynamics (AIMD) in combination with the temperature dependent effective potential (TDEP) method has been used to go beyond the quasiharmonic approximation and study the lattice dynamics in ceria, CeO<sub>2</sub>, at finite temperature. The results indicate that the previously proposed connection between the  $B_{1u}$  phonon mode turning imaginary and the transition to the superionic phase in fluorite structured materials is an artifact of the failure of the quasiharmonic approximation in describing the lattice dynamics at elevated temperatures. We instead show that, in the TDEP picture, a phonon mode coupling to the  $E_u$  mode prevents the  $B_{1u}$  mode from becoming imaginary. We directly observe the superionic transition at high temperatures in our AIMD simulations and find that it is initiated by the formation of oxygen Frenkel pairs (FP). These FP are found to form in a collective process involving simultaneous motion of two oxygen ions.

DOI: [10.1103/PhysRevB.97.104309](https://doi.org/10.1103/PhysRevB.97.104309)**I. INTRODUCTION**

Fluorite structured CeO<sub>2</sub>, or ceria, is a technologically important material for a wide range of applications, from oxygen storage to fuel cells. It has therefore been intensively studied for several decades [1,2]. One of the main focuses has been the high ionic conductivity, which is of importance for most areas of application. The ionic conductivity is directly related to the diffusion of oxygen ions through the material, usually via an oxygen vacancy hopping mechanism (VHM).

Oxygen vacancies can be introduced in pure ceria by chemical doping. Among the most common dopants are rare earth (RE) elements with lower valence than the Ce<sup>4+</sup> ions of the host material, for example Sm<sup>3+</sup> or Gd<sup>3+</sup>. Such doping facilitates fast ionic conductivity by the VHM and RE-doped ceria can, therefore, be used, for instance, as the electrolyte material in solid oxide fuel cells (SOFC) [2]. The vast majority of theoretical studies on the diffusion process and ionic conductivity in ceria has focused on the VHM.

Given that the operating temperature in most of the applications is rather high, surprisingly few studies have addressed the effect of temperature on the lattice dynamics in ceria. Several authors [3–5] have studied the phonon dispersion relations and related properties in ceria using the harmonic or quasiharmonic (QH) approximations that effectively disregard the anharmonic contributions to the lattice vibrations. To the best of our knowledge, the only study of the lattice dynamics in ceria beyond the QH approximation is the one of Niu *et al.* [6] who used the self-consistent *ab initio* lattice dynamical (SCAILD) method [7], which implicitly includes phonon-phonon interactions.

Another fact that has received little attention in connection to ceria is that fluorite and antiferroite structured materials

generally undergo a temperature induced (so-called type II) superionic phase transition. This is the transition to a state where the anions (or cations in the antiferroite materials) show a large degree of thermal disorder with high diffusivity, sometimes referred to as “sublattice melting.” The cations in the superionic phase remain well localized around their ideal face-centered cubic (fcc) positions. The superionic transition in fluorites typically occurs at a temperature  $T_c$  corresponding to  $\sim 80\%$  of the melting temperature ( $T_{\text{melt}} \approx 2750$  K for ceria [8]) and happens even in the absence of anion (cation) deficiency. This implies that the diffusion process in the superionic state cannot happen solely by uncorrelated vacancy hops. Instead, some diffusion process involving a collective rearrangement of anions (cations) needs to be present.

While  $T_c$  is much higher than the operation temperature in applications such as SOFCs, studying the superionic transition in ceria is of interest both fundamentally and for applied reasons. As it turns out, studying the superionic transition provides insight into the anharmonic lattice dynamics of ceria which is most likely transferable to other (anti)fluorite structured materials. Furthermore, it appears to be possible to reduce  $T_c$  substantially by applying moderate tensile strains, as was found for the fluorite structured materials CaF<sub>2</sub> and PbF<sub>2</sub> [9]. To explore other venues to further decrease  $T_c$  in ceria and related materials, insight into the mechanism of the superionic transition is clearly of importance.

Buckeridge *et al.* [5] have used the QH approximation to study the temperature dependence of the lattice dynamics in ceria. They proposed that a coupling between the  $B_{1u}$  and  $E_u$  phonon modes should lead to an increased probability of oxygen Frenkel pair (FP) formation. They also reported a softening of the  $B_{1u}$  phonon mode at the  $X$  point of the first Brillouin zone (BZ), which becomes imaginary at a temperature close to the superionic transition. That was interpreted as a transition to a thermally disordered phase. This imaginary mode has, in fact, been claimed to be responsible

\*johan.klarbring@liu.se

for the superionic transition in a large number of other fluorite and antifluorite structured materials [10–15].

It should be noted, however, that anharmonic effects beyond thermal expansion, i.e., beyond the QH approximation, are likely to become increasingly important on approaching a superionic transition, which is accompanied by highly anharmonic motion of the thermally disordered species. Furthermore, while the fact of the transition from a normal to superionic state is expected to be captured by a DFT based AIMD simulation, different exchange-correlation functionals will yield different equilibrium and thermally expanded lattice constants, making the transition temperature sensible to such a choice. Kovalenko *et al.* [16] have observed a superionic transition in their classical molecular dynamics (MD) studies of pure and Gd-doped ceria via a change in the activation energy of diffusion at high temperature and from studying the oxygen-oxygen radial distribution function.

In this paper we use the temperature dependent effective potential (TDEP) method, which is based on *ab initio* molecular dynamics (AIMD) with forces calculated within density functional theory (DFT), to study the lattice dynamics of stoichiometric ceria beyond the QH approximation. We pay particular attention to the superionic transition and show that the earlier reported connection between the softening of the  $B_{1u}$  mode at the  $X$  point of the first BZ and the superionic transition does not hold in ceria, being rather an artifact of the failure of the harmonic approximation at high temperature. We show that, in the TDEP picture, once the frequency of the  $B_{1u}$  mode decreases and matches the  $E_u$  mode frequency, these two modes couple, preventing the  $B_{1u}$  mode from becoming soft. At temperatures corresponding to the superionic transition we find spontaneous formation of O FPs, these are found to form in a collective manner, involving the simultaneous motion of two O ions. We argue that this collective FP formation is connected to the  $B_{1u}$  mode and suggest that the  $B_{1u} - E_u$  mode coupling may also be beneficial to the FP formation.

## II. METHODOLOGY

### A. The temperature dependent effective potential method

The TDEP method [17,18] uses forces and atomic displacements generated from AIMD to fit effective interatomic force constants (IFCs). We use a model Hamiltonian of the form:

$$H = U_0 + \sum_i \frac{\mathbf{p}_i^2}{2m_i} + \sum_{i,j} \mathbf{u}_i^T \Phi_{ij} \mathbf{u}_j, \quad (1)$$

where  $m_i$  is the mass,  $\mathbf{p}_i$  the momentum, and  $\mathbf{u}_i$  the displacement from equilibrium of atom  $i$ .  $U_0$  is a constant potential energy term and  $\Phi_{ij}$  are the second order IFCs that will be fitted.

Given sets of forces  $\{\mathbf{F}_i\}$  and corresponding atomic displacements  $\{\mathbf{u}_i\}$  from AIMD, the IFCs  $\Phi_{ij}$  are extracted by a least squares minimization of the difference between the AIMD forces and the forces generated from the IFCs. This minimization is constrained to impose the symmetry of the underlying lattice onto  $\Phi_{ij}$ . The TDEP procedure thus generates IFCs that are explicit functions of the fixed external parameters (e.g., volume and temperature) of the AIMD simulation and, since they are fitted directly from AIMD data, they contain

renormalized anharmonicity to all orders. In this paper, the atomic displacements,  $\{\mathbf{u}_i\}$ , are taken with respect to the ideal fluorite positions at all temperatures. Since the model Hamiltonian is of second order it can be diagonalized and hence there exist well defined phonon quasiparticles. Related quantities, such as phonon dispersion relations, density of states (DOS) and free energies can thus be calculated in a straightforward way.

TDEP has been successfully used to describe finite temperature lattice dynamics and phase stability in materials of various sorts, see for instance Refs. [19,20].

### B. Computational details

All density-functional theory (DFT) calculations were performed using the projector augmented wave (PAW) [24] method as implemented in the Vienna *ab initio* simulation package (VASP) [25–27]. Exchange and correlation effects were treated using the PBEsol [28] form of the generalized gradient approximation (GGA), which yields the 0 K equilibrium volume of 5.40 Å<sup>3</sup>, in good agreement with experimental values [21,22,29]. We choose not to apply a Hubbard  $U$  term, commonly used in calculations of ceria based materials to compensate for the poor description of the ceria  $4f$  state in standard DFT. Such a correction is not needed in the present case since we treat perfectly stoichiometric ceria where the  $4f$  states of Ce are not occupied [30]. Indeed, applying a standard value of  $U = 5$  eV [30] makes the PBEsol equilibrium lattice constant, 5.431 Å [5], deviate further from experiment.

The Kohn-Sham orbitals were expanded in plane waves up to a kinetic energy cutoff of 600 eV. We used PAW potentials which treat the Ce  $4s4p4f5d6s$  and the O  $2s2p$  electrons as valence. The calculations were not spin polarized, this is motivated by the fact that we treat perfectly stoichiometric ceria where the electronic DOS is identical for the spin up and spin down channels [30]. Born-Oppenheimer AIMD simulations were performed in the NVT ensemble using a Nosé-Hoover thermostat [31,32] with the default Nose mass as set by VASP and a 2 fs timestep. Simulations were at least 12 ps long, and an equilibration period of 1 ps was disregarded before any data was gathered.

The temperature dependence of the cubic lattice constant  $a(T)$  was extracted by running AIMD simulations using a 96 atom supercell on a grid of seven temperatures from 300 to 2100 K in steps of 300 K and three volumes at each temperature. The equilibrium volume was found by an interpolation to zero pressure using the third-order Birch-Murnaghan equation of state [33].

Temperature dependent phonon dispersion relations and DOS were extracted using the TDEP method (see Sec. II A) and static, 0 K, phonon dispersion relations were calculated using the small displacement method [34] as implemented in the PHONOPY [35] software package, using the default displacement distance 0.01 Å. All phonon calculations were performed in a supercell constructed as a  $4 \times 4 \times 4$  repetition of the primitive three atom fcc unit cell, 192 atoms in total. The BZ sampling was limited to the  $\Gamma$  point for the AIMD simulations, while a  $3 \times 3 \times 3$  Monkhorst-Pack grid was used for the static phonon calculations.

The LO-TO splitting (where LO and TO stand for the longitudinal and transverse optical modes, respectively) affects only the  $F_{1u}$  LO-TO modes of ceria. It has no effect on the  $B_{1u}$  and  $E_u$  modes that are of primary importance to this paper and in no way influence the presented conclusions. Therefore the LO-TO splitting was not taken into account.

### III. RESULTS AND DISCUSSION

#### A. Finite temperature lattice dynamics in ceria

Our calculated lattice constants are shown in Fig. 1; we find that they agree very well with experimental results [21,22], with just a slight overestimation. The top left panel of Fig. 2 shows the  $\text{CeO}_2$  phonon dispersion relations along certain high symmetry directions of the first BZ calculated using the TDEP method at 300 K, compared to room temperature inelastic neutron diffraction data from Ref. [23]. We note that the agreement is fairly good, especially in the low and intermediate frequency range.

Figure 2 also contains the TDEP dispersion relations and DOS at 900, 1500, and 2100 K. Apart from a general softening of the frequency across all phonon branches, the most distinct change with increasing temperature is found for the  $B_{1u}$  mode at the X point, which softens considerably faster than most other modes. Note that it has passed the  $E_u$  mode at 2100 K. Associated with the  $B_{1u}$  mode at the X point is a peak in the oxygen phonon DOS, marked with horizontal lines in the DOS at 1800 and 2100 K (Fig. 2), which indicates a high population of this and its neighboring modes.

The  $B_{1u}$  mode consists of displacements of alternating (110) planes of the oxygen sublattice in the positive and negative [001] direction. The twofold degenerate  $E_u$  mode displaces both Ce and O ions; the O and Ce movements are orthogonal

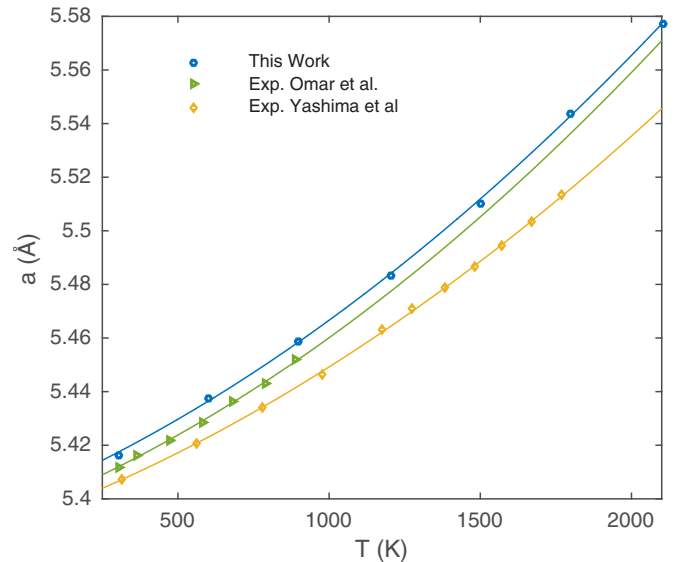


FIG. 1. Temperature dependence of the  $\text{CeO}_2$  cubic lattice parameter  $a$ , as calculated from AIMD in this work and from experiment [21,22]. The lines are fits to second order polynomials.

to each other and to the  $B_{1u}$  mode. The detailed displacements are shown in Fig. 3.

In the quasiharmonic approximation the  $B_{1u}$  mode has been found to turn imaginary at temperatures around the superionic transition in ceria [5] and several other materials with fluorite and antifluorite structures [10–15]. Motivated by this fact we have, in addition to the TDEP simulations, calculated static phonon dispersions at volumes from the 0 K equilibrium volume up to 5% increased volume, i.e., applying up to 5% isotropic tensile strain. These volumes are assigned

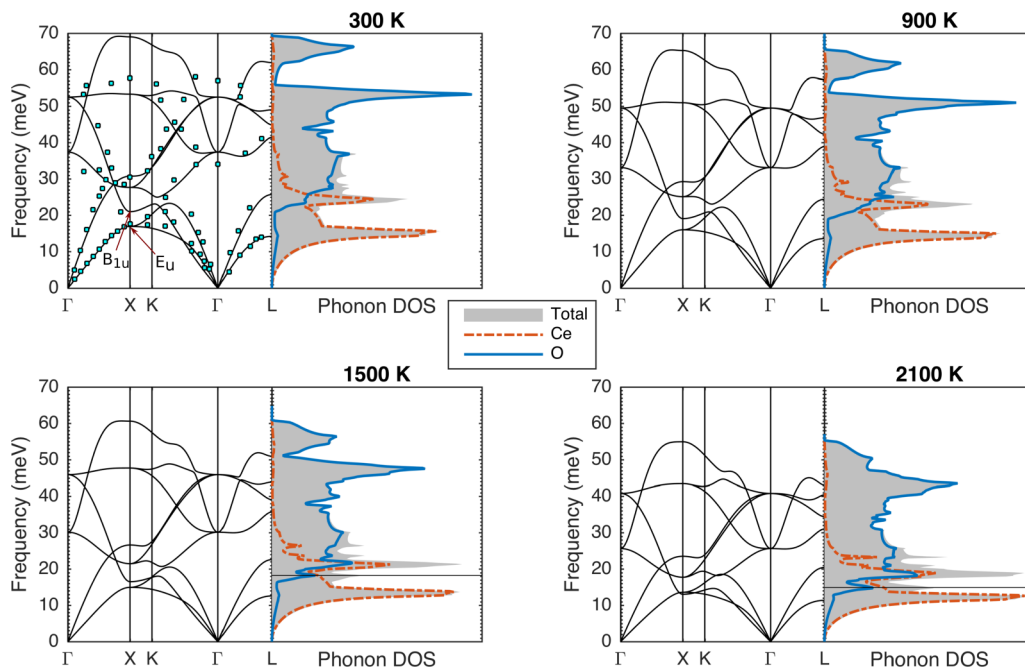


FIG. 2. Phonon dispersion relations calculated using the TDEP method at 300, 900, 1500, and 2100 K. The 300 K dispersion is compared to inelastic neutron scattering data (squares) [23]. Horizontal lines in the phonon DOS mark the appearance of a peak in the low frequency part of the oxygen partial DOS.

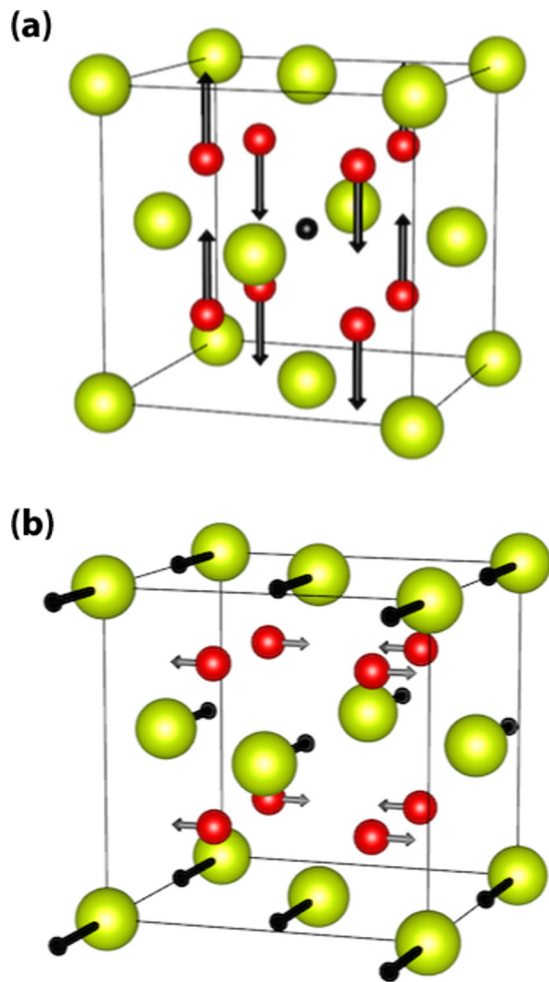


FIG. 3. (a) Atomic displacements of the  $B_{1u}$  phonon mode at the  $X$  point. Alternating (110) planes of the O ions move in opposite directions along the [001] direction. (b) Atomic displacements of the  $E_u$  phonon mode at the  $X$  point, with the O and Ce moving orthogonally to each other and to the  $B_{1u}$  mode. The  $E_u$  mode is twofold degenerate; the displacements of the second mode are found by rotating the first one by 90 degrees around the [001] direction. Green and red spheres represent Ce and O ions, respectively. The octahedral interstitial site is shown as a black sphere in (a).

a temperature using the calculated temperature-volume scale from Fig. 1.

Following Buckeridge *et al.* [5] we focus on the  $B_{1u}$  and  $E_u$  mode at the  $X$  point. Figure 4 shows the temperature dependence of the frequencies, as obtained from both static and TDEP calculations. We find that the static and TDEP phonon frequencies are rather close at low temperatures but start to deviate substantially at higher temperatures. The deviation is more drastic for the  $B_{1u}$  but distinctly present also for the  $E_u$  mode. This is a clear indication that the effective, temperature dependent, potential energy surface substantially deviates from the quasiharmonic one at high temperatures. In the AIMD simulations at and above  $T_c = 2150$  K we observed a nonzero slope of the mean squared displacement (MSD) among the oxygen ions (see Fig. 5), indicating that they undergo a net displacement during the simulations. The Ce ions were found to vibrate around their ideal equilibrium positions,

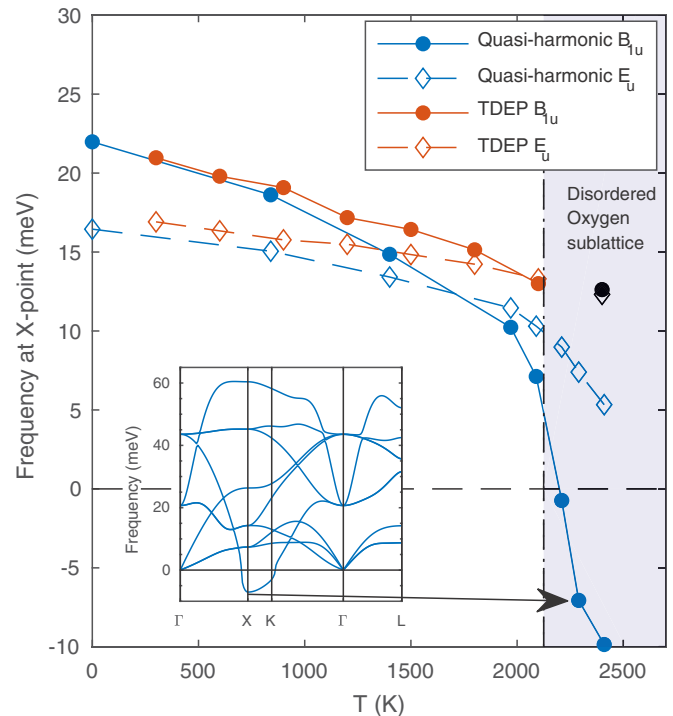


FIG. 4. Frequency of the  $B_{1u}$  (circles and solid lines) and  $E_u$  modes (diamonds and dashed lines) at the  $X$  point as calculated using TDEP (red and black) and QH (blue) vs temperature. The inset shows the QH phonon dispersion at a volume corresponding to 2300 K. The vertical line at 2150 K corresponds to the superionic transition temperature  $T_c$ .

and correspondingly a flat profile of the Ce MSD was seen. We note that since there are no oxygen vacancies present in the supercell, the diffusion of the oxygen ions cannot happen through the normal vacancy hopping process. We treat  $T_c$  as the critical temperature of the superionic transition [36].

We see, as noted above, that  $T_c$  is close to the temperature where the  $B_{1u}$  mode frequency at the  $X$  point becomes imaginary in the QH approximation. We also see, however, that the TDEP results show that this instability is not present when anharmonic effects are properly taken into account. Instead, we note that  $T_c$  closely correlates with the temperature at which the  $B_{1u}$  and  $E_u$  modes cross in the TDEP picture. We can thus conclude that the proposed connection between the superionic transition and the imaginary  $B_{1u}$  mode is not as clear as previously suggested. This result is likely valid not only for ceria but also for other (anti)fluorite structured materials.

Since the O ions no longer keep their ideal equilibrium positions above  $T_c$ , the standard phonon picture breaks down. As will be discussed below, the diffusion process above  $T_c$  is found to consist of discrete correlated events. In between these diffusion events the system returns to the ideal fluorite structure. This makes it possible to associate each atom with a particular fluorite lattice site for times between the diffusion events. The corresponding displacement from these lattice sites  $\{\mathbf{u}_i\}$ , needed in the TDEP method, can thus be identified. We then use only the timesteps where this identification can be safely made to extract the IFCs and subsequently the phonon frequencies using TDEP.

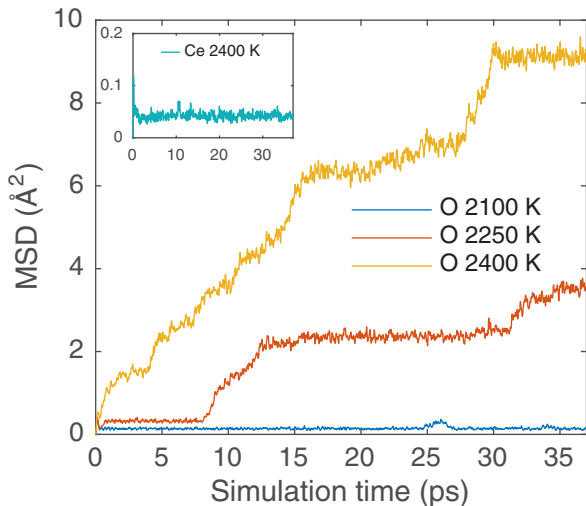


FIG. 5. Mean squared displacement (MSD)  $(1/N) \sum_i (\mathbf{r}_i(0) - \mathbf{r}_i(t))^2$  of O ions as a function of simulation time;  $N$  is the number of ions  $\mathbf{r}_i(t)$  is the position of ion  $i$  at time  $t$ . The nonzero slope of the MSD for temperatures 2250 and 2400 K indicates nonzero diffusion among the O ions and thus the system is in the superionic state. The inset shows the MSD for Ce ions at 2400 K; here the slope of the MSD is zero, indicating that the Ce ions keep their ideal equilibrium positions.

This procedure is carried out at 2400 K and the corresponding  $B_{1u}$  and  $E_u$  mode frequencies are given by the stand alone black symbols in Fig. 4. We now see that after the  $B_{1u}$  and  $E_u$  modes cross around 2100 K the  $B_{1u}$  mode does not continue to decrease at the same rate but instead sticks to the  $E_u$  mode. This may indicate that for temperatures above the crossing there is a strong anharmonic coupling between the two modes.

To further investigate the possibility of a mode coupling we note that it should be possible to make the two modes cross at temperatures lower than 2100 K by applying expansive strain. If the coupling mechanism is present in the system, the two modes should decrease at the same rate with increasing volume once the frequencies have crossed, provided that the temperature is high enough.

The TDEP method generates IFCs that are explicit functions of the fixed external parameters of the AIMD simulation, in our case volume and temperature, i.e.,  $\Phi_{ij}^{TDEP} = \Phi_{ij}^{TDEP}(V, T)$ , while the QH method yields IFC's that are explicitly volume dependent and only implicitly depend on temperature through a temperature dependent volume, i.e.,  $\Phi_{ij}^{QH} = \Phi_{ij}^{QH}(V(T))$ . Because of this, the TDEP method can, as opposed to the QH method, be used to study how the lattice vibrations are affected by volume changes at different fixed temperatures. This is, in fact, an interesting topic in itself since expansive strain has been studied intensively in recent years as a way to enhance the ionic conductivity in ceria and other fast ionic conductors [37–42].

For simplicity we focus on isotropic strain, but we note that it is biaxial strain that is commonly realized in experimental studies. Figure 6 displays the frequencies of the  $B_{1u}$  and  $E_u$  modes for isotropic strains,  $\epsilon$  from  $-2$  to  $5\%$  at 0, 300, 900, and 1500 K. At 0 and 300 K the two modes decrease with increasing volume at different rates and no clear coupling between them can be seen. On the other hand at 900 K and 1500 K, once

the modes cross (at  $\epsilon \approx 2$  and  $1\%$ , respectively) they start to decrease at the same rate. This provides further evidence of a coupling between the two phonon modes.

We can summarize this result as follows: Once the  $B_{1u}$  mode decreases in frequency, by increasing the temperature or volume, so that it crosses the  $E_u$  mode, anharmonic effects make the two modes couple, and they subsequently decrease at the same rate. This occurs provided that the temperature is high enough so that the anharmonic effects are sufficiently strong.

We thus expect a large degree of in-phase movement of these two modes at high temperature or volume. We will discuss below how this may be related to the superionic transition.

## B. Superionic transition

As we noted in the previous section, for temperatures above  $T_c = 2150$  K the O ions are found to rather rapidly diffuse through the lattice. Such a transition to a phase with a thermally disordered oxygen sublattice is known as a type-II superionic transition [43], which is common in materials with the fluorite (antifluorite) structure. A large degree of disorder is induced among the anions (cations) while the cations (anions) stay around their ideal fcc positions.

From a more careful investigation of the atomic trajectories from the AIMD simulations above  $T_c$ , we find that the diffusion mainly consists of separated, collective, events. In between these diffusion events the system retains the perfect fluorite structure.

These diffusion events are found to be initiated by the formation of oxygen Frenkel pairs, i.e., the combination of an O vacancy and O interstitial. The interstitial site is in the center of the octahedron formed by six Ce ions, or equivalently in the center of the cube formed by 8 O ions, as depicted in Fig. 3(a). We find that these FP's are formed through a collective mechanism involving two O ions: When one O ion moves away from its ideal lattice site towards the octahedral interstitial site, one of its neighboring O ions simultaneously moves to take its place. This results in a stable O interstitial with eight nearest neighbor (NN) O ions. This collective movement of two O ions is needed to form a stable FP since the simplest FP, i.e., the O interstitial and the vacancy as NN, is unstable w.r.t. the recombination of the interstitial into the vacancy, as has been previously noted in static calculations [44]. The formation of such a FP effectively generates a vacancy in the O sublattice which can facilitate further diffusion of O ions through vacancy hopping. Once the vacancy hopping generates a vacancy among one of the eight NNs of the interstitial O ion, the interstitial may move into this vacant site and the perfect lattice is recovered. The net movement of the interstitial O is thus either zero if it moves back to its original site, or it is in the [100], [110], or [111] type directions from its original site, as shown in Figs. 7(a)–7(d) for 2250 K. From Fig. 7 one can also see that a typical lifetime of an oxygen FP is of the order of 1 ps. An example of such a collective diffusion event is shown schematically in Fig. 8.

We note that these collective events form closed loops, which means that they cannot give a net contribution to the ionic conductivity. It is likely, however, that such collective diffusion events have a net positive influence on the ionic conductivity if O vacancies are present in the system, as, e.g.,

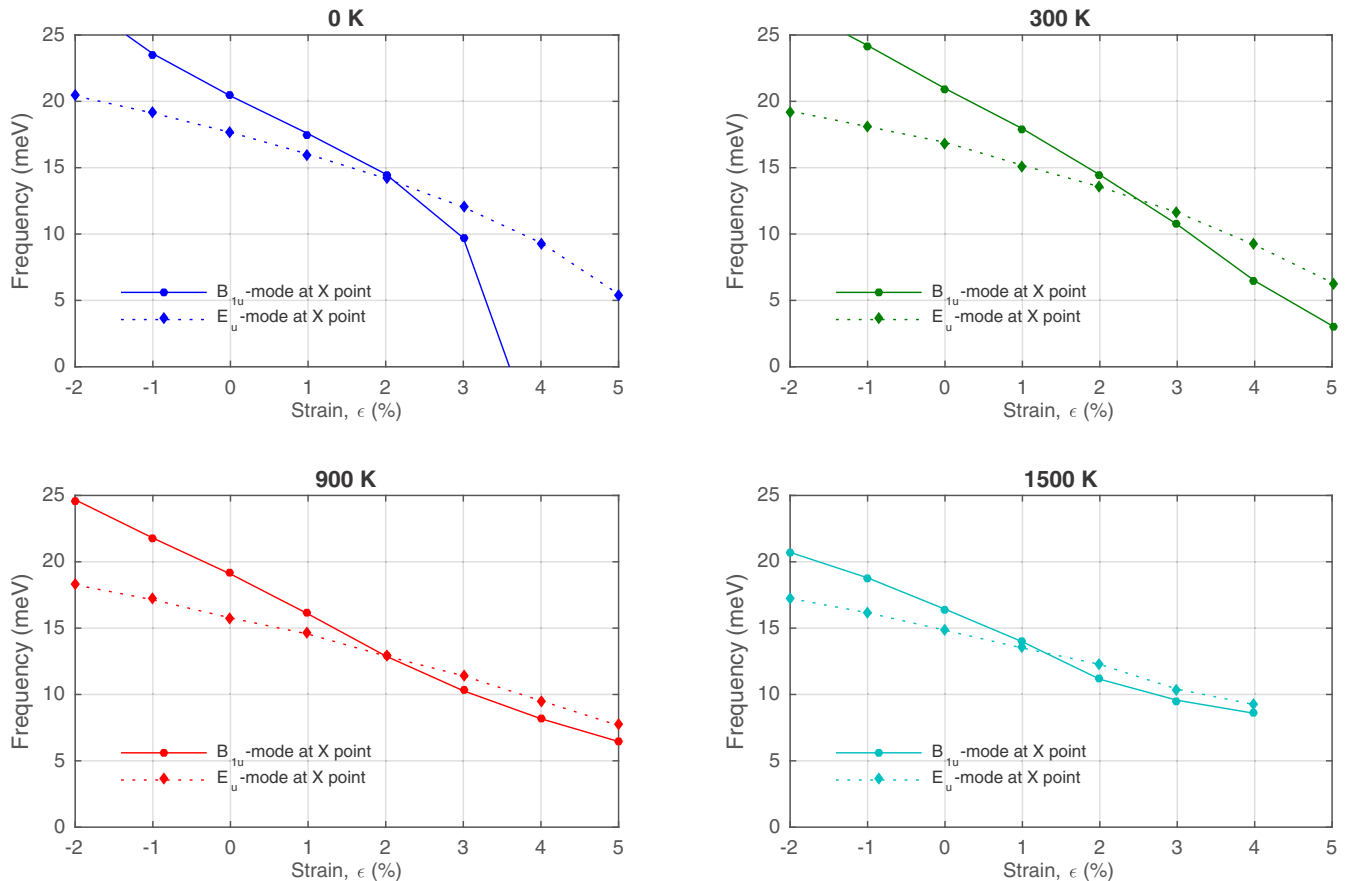


FIG. 6. Frequency of the  $B_{1u}$  (dot markers and solid lines) and  $E_u$  modes (diamond markers and dotted lines) as a function of isotropic strain at 0, 300, 900, and 1500 K.

in RE doped ceria. Buckeridge *et al.* [5] proposed a similar conduction mechanism, also facilitated by the O interstitials. This mechanism was then used to explain the experimental observation of Hohnke [45] that the ionic conductivity of Gd-doped ceria samples with different dopant concentration appears to converge to the same value above  $\sim 1600$  K. Since the O vacancy concentration follows the Gd concentration, this could imply that a conduction mechanism other than a simple VHM is present above this temperature. We note that the conduction mechanism we propose, i.e., the O FPs effectively creating O vacancies in the lattice, should be less dependent on the concentration of the O vacancies than the VHM. Buckeridge *et al.* connected the temperature, at which the convergence of the conductivities at different concentrations of dopants occur, to the temperature where the  $B_{1u}$  and  $E_u$  modes cross in their QH calculations. As we will discuss in the next section, the connection between the formation of the O FPs and the crossing of these modes is not that clear in the TDEP picture.

### C. Discussion: Connection between Frenkel Pair formation and the $B_{1u}$ and $E_u$ modes

As we have noted above, the connection between the superionic transition (caused by an increased rate of FP formation) and the complete softening (i.e., an imaginary

frequency) of the  $B_{1u}$  mode is an artifact of the failure of the QH approximation as the critical temperature of the superionic transition is approached. At high temperatures the  $B_{1u}$  mode is, however, still the lowest frequency mode, apart from the acoustic modes, containing any appreciable O motion and is thus expected to play a dominant role in the dynamics of the O ions. We therefore point out that the observed collective nature of the FP formation can be straightforwardly related to the  $B_{1u}$  mode when the atomic displacements in this mode are viewed as the collective movements of chains of O ions along a [100] direction (see Fig. 3).

As previously mentioned, Buckeridge *et al.* [5] proposed that a coupling between the  $B_{1u}$  and  $E_u$  phonon modes should lead to an increased probability of the oxygen FP formation since the net O movement of the three modes (singlet  $B_{1u}$  and doublet  $E_u$ ) is towards the octahedral interstitial site. In the QH approximation the ratio of the Ce to O amplitude of motion in the  $E_u$  mode is  $\sim 15$  at 0 K, i.e., the mode is completely dominated by the Ce motion. At 2200 K this ratio is  $\sim 3$ , so that the O motion, although significantly smaller than the Ce motion, is non-negligible.

In the TDEP picture, however, this ratio is  $\sim 8$  at 2100 K, indicating that, counterintuitively, explicit anharmonic effects (other than the volume expansion), in fact, increase the Ce motion relative to the O motion in the  $E_u$  mode, to the extent that this mode is completely dominated by the Ce motion even

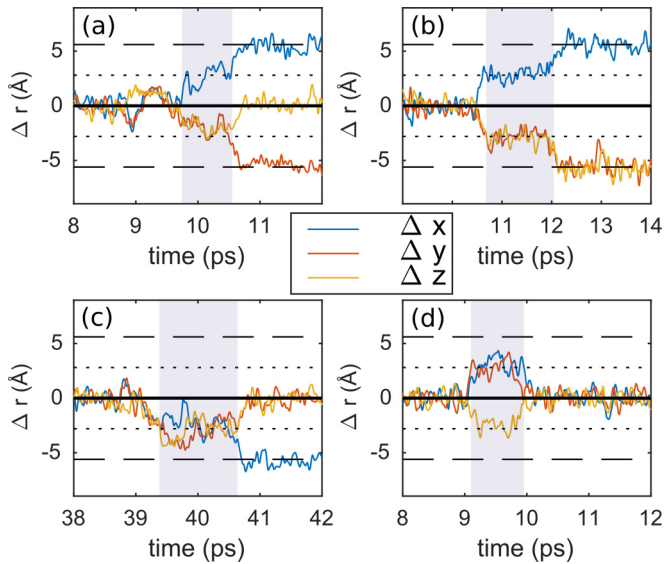


FIG. 7. Deviations of  $x$ ,  $y$ , and  $z$  coordinates of four selected O ions from equilibrium ( $\Delta x$ ,  $\Delta y$ , and  $\Delta z$ , respectively). The AIMD simulation is performed at  $T = 2250$  K. The dashed lines mark the distance to a neighboring O site, while the dotted lines mark coordinates of the octahedral interstitial site. The shaded areas highlight the formation of Frenkel pairs (FP), i.e., when the O ion occupies the octahedral interstitial site and its original lattice site is vacant. The four figures show the four possible simple recombination processes of the O interstitial, i.e., where the O ion forming the FP ends up in a lattice site in a (a) [110], (b) [111], (c) [100] type direction and (d) returns to its initial site.

at temperatures around the superionic transition. This makes the connection between FP formation and the  $B_{1u}$  and  $E_u$  mode coupling unclear. We note, however, that the total atomic motion at these temperatures is much larger among the O ions than among the Ce ions, in spite of the fact that the  $E_u$  modes are dominated by the Ce motion.

#### IV. SUMMARY AND CONCLUSION

In summary we have studied the finite temperature lattice dynamics in ceria using the TDEP method. As expected, the TDEP description starts to deviate from the QH approximation as temperature increases. In particular, the  $B_{1u}$  mode at the  $X$  point becomes imaginary in the QH picture at  $\sim 2300$  K, while such a softening is not observed in the TDEP calculations. We thus conclude that the proposed connection between the critical softening of this mode and the superionic transition is not accurate but is instead a result of the failure of the (quasi)harmonic approximation at high temperatures.

Instead, in the TDEP picture the  $B_{1u}$  mode decreases with temperature at a certain rate until it crosses the frequency of the  $E_u$  mode, after which these two modes further decrease with temperature at the same rate. Similar behavior of the two modes is observed when they are made to cross by expanding the volume, provided that the temperature is also high enough. We interpret this as a coupling between the two modes which prevents the  $B_{1u}$  mode from becoming soft.

In our AIMD simulations at temperatures above 2100 K we found spontaneous formation of oxygen Frenkel Pairs (FP).

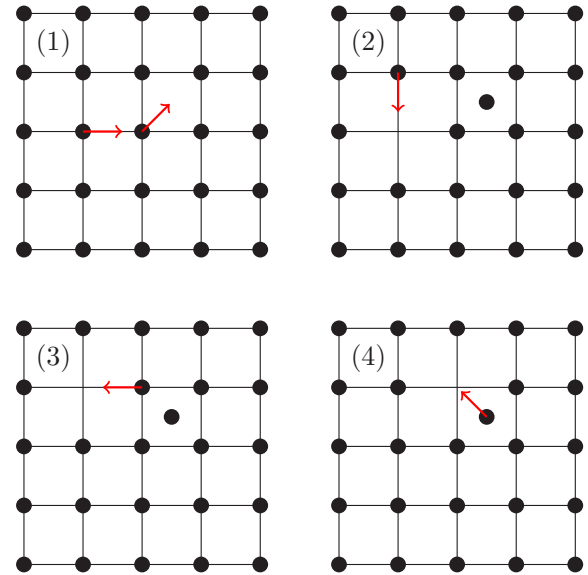


FIG. 8. Cartoon illustration of one possible simple collective diffusion process involving an O Frenkel pair (FP): (1): An O FP is formed from a collective process involving two O ions, leaving a vacancy in the system. (2) and (3): This allows for a neighboring O ions to diffuse into the vacant sites, (4): Once one of the O interstitial nearest neighbor lattice site becomes vacant the interstitial ion moves into this site, and the perfect lattice is recovered.

These FP are found to form via a collective process involving two O ions, ending in an O interstitial surrounded by eight nearest neighbor O ions. This is necessitated by the fact that the O interstitial with seven neighbors, i.e., simply moving one O from its ideal site to the interstitial, is unstable with respect to the return of the oxygen ion into its original position. The formation of such a FP effectively leaves an O vacancy in the system into which neighboring O ions can migrate.

We finally noted that the collective formation of FPs is likely connected to the atomic displacements of the  $B_{1u}$  mode. The connection between the coupling of the  $B_{1u}$  and  $E_u$  modes and the FP formation, proposed on the basis of the QH approximation, is however, not directly supported by our TDEP calculations, since in the TDEP picture, the  $E_u$  mode is completely dominated by Ce motion.

#### ACKNOWLEDGMENTS

The support from Swedish Research Council (VR) (Project No. 2014-4750) and the Swedish Government Strategic Research Area in Materials Science on Functional Materials at Linköping University (Faculty Grant SFO-Mat-LiU No. 2009 00971) are acknowledged by S.I.S. and J.K. N.V.S. acknowledges the financial support of the Swedish Research Council (VR) (Project No. 2014-5993). The computations were performed on resources provided by the Swedish National Infrastructure for Computing (SNIC) at the PDC Centre for High Performance Computing (PDC-HPC) and the National Supercomputer Center (NSC).

- [1] A. Trovarelli, *Catal. Rev.* **38**, 439 (1996).
- [2] D. J. L. Brett, A. Atkinson, N. P. Brandon, and S. J. Skinner, *Chem. Soc. Rev.* **37**, 1568 (2008).
- [3] Y. Wang, L. A. Zhang, S. Shang, Z.-K. Liu, and L.-Q. Chen, *Phys. Rev. B* **88**, 024304 (2013).
- [4] T. Gürel and R. Eryiğit, *Phys. Rev. B* **74**, 014302 (2006).
- [5] J. Buckeridge, D. O. Scanlon, A. Walsh, C. R. A. Catlow, and A. A. Sokol, *Phys. Rev. B* **87**, 214304 (2013).
- [6] Z.-W. Niu, Z.-Y. Zeng, C.-E. Hu, L.-C. Cai, and X.-R. Chen, *J. Chem. Phys.* **142**, 014503 (2015).
- [7] P. Souvatzis, O. Eriksson, M. I. Katsnelson, and S. P. Rudin, *Phys. Rev. Lett.* **100**, 095901 (2008).
- [8] M. Mogensen, N. M. Sammes, and G. A. Tompsett, *Solid State Ionics* **129**, 63 (2000).
- [9] C. Cazorla and D. Errandonea, *Nano Lett.* **16**, 3124 (2016).
- [10] C. Cazorla and D. Errandonea, *Phys. Rev. Lett.* **113**, 235902 (2014).
- [11] M. K. Gupta, P. Goel, R. Mittal, N. Choudhury, and S. L. Chaplot, *Phys. Rev. B* **85**, 184304 (2012).
- [12] L. Boyer, *Phys. Rev. Lett.* **45**, 1858 (1980).
- [13] L. Boyer, *Solid State Ionics* **5**, 581 (1981).
- [14] L. Zhou, J. Hardy, and H. Cao, *Solid State Commun.* **98**, 341 (1996).
- [15] R. Fracchia, G. Barrera, N. Allan, T. Barron, and W. Mackrodt, *J. Phys. Chem. Solids* **59**, 435 (1998).
- [16] M. Kovalenko and A. Y. Kupryazhkin, *J. Nucl. Mater.* **430**, 12 (2012).
- [17] O. Hellman, I. A. Abrikosov, and S. I. Simak, *Phys. Rev. B* **84**, 180301 (2011).
- [18] O. Hellman, P. Steneteg, I. A. Abrikosov, and S. I. Simak, *Phys. Rev. B* **87**, 104111 (2013).
- [19] L. Burakovsky, N. Burakovsky, M. J. Cawkwell, D. L. Preston, D. Errandonea, and S. I. Simak, *Phys. Rev. B* **94**, 094112 (2016).
- [20] N. Shulumba, Z. Raza, O. Hellman, E. Janzén, I. A. Abrikosov, and M. Odén, *Phys. Rev. B* **94**, 104305 (2016).
- [21] S. Omar, E. D. Wachsman, J. L. Jones, and J. C. Nino, *J. Am. Ceram. Soc.* **92**, 2674 (2009).
- [22] M. Yashima, D. Ishimura, Y. Yamaguchi, K. Ohoyama, and K. Kawachi, *Chem. Phys. Lett.* **372**, 784 (2003).
- [23] K. Clausen, W. Hayes, J. E. Macdonald, R. Osborn, P. G. Schnabel, M. T. Hutchings, and A. Magerl, *J. Chem. Soc., Faraday Trans. 2* **83**, 1109 (1987).
- [24] P. E. Blöchl, *Phys. Rev. B* **50**, 17953 (1994).
- [25] G. Kresse and D. Joubert, *Phys. Rev. B* **59**, 1758 (1999).
- [26] G. Kresse and J. Furthmüller, *Comput. Mater. Sci.* **6**, 15 (1996).
- [27] G. Kresse and J. Furthmüller, *Phys. Rev. B* **54**, 11169 (1996).
- [28] J. P. Perdew, A. Ruzsinszky, G. I. Csonka, O. A. Vydrov, G. E. Scuseria, L. A. Constantin, X. Zhou, and K. Burke, *Phys. Rev. Lett.* **100**, 136406 (2008).
- [29] T. Hisashige, Y. Yamamura, and T. Tsuji, *J. Alloys Compd.* **408-412**, 1153 (2006).
- [30] D. A. Andersson, S. I. Simak, B. Johansson, I. A. Abrikosov, and N. V. Skorodumova, *Phys. Rev. B* **75**, 035109 (2007).
- [31] S. Nosé, *J. Chem. Phys.* **81**, 511 (1984).
- [32] W. G. Hoover, *Phys. Rev. A* **31**, 1695 (1985).
- [33] F. Birch, *Phys. Rev.* **71**, 809 (1947).
- [34] D. Alfè, *Comput. Phys. Commun.* **180**, 2622 (2009).
- [35] A. Togo and I. Tanaka, *Scr. Mater.* **108**, 1 (2015).
- [36] Conventionally, the critical temperature of the superionic transition is taken at the temperature corresponding to the top of the so-called  $\lambda$  peak in the heat capacity. The onset of the disorder sets in at slightly lower temperatures. This distinction is unimportant in the present context and for simplicity we identify  $T_c$  with the onset of disorder among the O ions.
- [37] M. Alaydrus, M. Sakaue, S. M. Aspera, T. D. K. Wungu, N. H. Linh, T. P. T. Linh, H. Kasai, T. Ishihara, and T. Mohri, *J. Phys. Soc. Jpn.* **83**, 094707 (2014).
- [38] K. Wen, W. Lv, and W. He, *Journal of Materials Chemistry A* **3**, 20031 (2015).
- [39] T. J. Pennycook, M. J. Beck, K. Varga, M. Varela, S. J. Pennycook, and S. T. Pantelides, *Phys. Rev. Lett.* **104**, 115901 (2010).
- [40] M. Rushton, A. Chroneos, S. Skinner, J. Kilner, and R. Grimes, *Solid State Ionics* **230**, 37 (2013).
- [41] M. J. D. Rushton and A. Chroneos, *Sci. Rep.* **4**, 6068 (2014).
- [42] A. Fluri, D. Pergolesi, V. Roddatis, A. Wokaun, and T. Lippert, *Nat. Commun.* **7**, 10692 (2016).
- [43] S. Hull, *Rep. Prog. Phys.* **67**, 1233 (2004).
- [44] T. Zacherle, A. Schriever, R. A. De Souza, and M. Martin, *Phys. Rev. B* **87**, 134104 (2013).
- [45] D. Hohnke, *Solid State Ionics* **5**, 531 (1981), proceedings of the International Conference on Fast Ionic Transport in Solids.